file:///Z|/TPB/REPLACE/437.htm

National Weather Service
Office of Meteorology

Technical Procedures Bulletin

Subject:

AIRCRAFT ICING FORECASTS FOR THE CONTIGUOUS UNITED STATES

Series No. 437

Program Requirements and Development Division, Silver Spring, MD 20910

This bulletin, written by Ronald M. Reap of the Techniques Development Laboratory, describes the new NGM-based MOS 6-h aircraft icing index forecasts for the contiguous U.S. that have been produced daily for the National Centers of Environmental Prediction's (NCEP's) Aviation Weather Center (AWC) and Hydrometeorological Prediction Center (HPC) since early 1997.

The forecast equations were developed from forecast fields from the NCEP's Nested Grid Model (NGM) (Hoke et al. 1989), national lightning location data (Krider et al. 1976), and pilot reports (PIREPS) from the AWC's data archives. This TPB is the first to describe the new forecast products for predicting aircraft icing. The forecasts were designed to provide general objective guidance in the 2-26 h timeframe to forecasters at AWC and HPC. AWC is responsible for issuing operational AIRMETS and SIGMETS which are inflight advisories for use by the aviation community.

The new forecasts are valid for the 2-8 h, 8-14 h, 14-20 h, and 20-26 h projections after 0000 and 1200 UTC initial data times. They predict the occurrence of category 4 (light-to-moderate) or greater aircraft icing for grid blocks that are 48-km on a side. Separate forecasts are produced for the high-band (> 15,000 ft AGL) and low-band (< 15,000 ft AGL) regions.

Full HTML Text or PDF format .

LeRoy Spayd
Chief, Training and Professional Development Core

U.S.DEPARTMENT OF COMMERCE **National Oceanic and Atmospheric Administration**

file:///V|/TPB/REPLACE/437body.htm

AIRCRAFT ICING FORECASTS FOR THE CONTIGUOUS U.S.

by Ronald M. Reap, Techniques Development Laboratory

1. INTRODUCTION

This bulletin describes the new NGM-based MOS forecasts of nonconvective aircraft icing for the contiguous U.S. that were operationally implemented during the 1996-97 cool season. The equations to produce these forecasts were developed from forecast fields from the National Centers for Environmental Prediction's (NCEP's) Nested Grid Model (NGM) (Hoke et al. 1989), national lightning location data (Krider et al. 1976), and pilot reports (PIREPS) from the Aviation Weather Center's (AWC's) data archives. The forecast equations predict the probability of occurrence of category 4 (light-to-moderate) or greater aircraft icing in 48-km grid blocks covering the contiguous U.S. during 6-h periods that are valid 2-8, 8-14, 14-20, and 20-26 hours after 0000 and 1200 UTC initial data times. The new icing forecasts were designed to provide general objective guidance in the 2-26 h timeframe to forecasters at the Aviation Operations Branch of AWC located in Kansas City, MO. AWC is responsible for issuing operational inflight advisories (AIRMETS and SIGMETS) for use by the aviation community.

2. DEVELOPMENT

a. Method

The icing forecast equations were derived by applying screening regression techniques and the Model Output Statistics (MOS) approach (Glahn and Lowry 1972) to relate the PIREP predictand data to large-scale meteorological predictors obtained from the NGM. National lightning location data were used to eliminate icing reports arising from localized thunderstorm activity. As a result, the forecast equations predict the probability of occurrence of nonconvective aircraft icing. Separate equations were developed for the eastern and western U.S. (Fig. 1) to accommodate the unique meteorological conditions related to icing over the western mountains. Equations were developed for the high-band (15,000 ft above ground level (AGL)) and low-band (< 15,000 ft AGL) regions. Separate forecast equations were also developed for the warm season (March 16 - September 30) and cool season (October 1 - March 15) periods.

b. Predictand Sample

PIREP data were obtained from AWC for the three-year period from 1988-90. Like many observed datasets, PIREPS suffer from specific limitations (Schwartz 1996). They are, however, the only practical method for determining the existence of aircraft icing. The reports are intermittent in both space and time and are relatively scarce at night when few aircraft are aloft. Reports of icing are subjective in nature and, therefore, uncalibrated since they depend upon the pilot's perception of the degree of icing. Despite this limitation, the present developmental effort was successful in using the PIREPS to identify significant areas of aircraft icing that were related to major features in the large-scale flow.

During initial processing, the reported icing events, whose positions are given by latitude and longitude in the PIREPS, were related to an 89x113 grid covering the contiguous U.S. (Fig. 1). The maximum value of icing observed during the hour was tabulated and stored for each 48-km grid block in the 89x113 array, i.e., if multiple icing events were reported for an individual 48-km grid block, only the maximum value was saved. The archived icing intensity for each grid block was indicated by the category values that were originally used to encode the PIREPS, i.e.,

- 0 = None

file:///V|/TPB/REPLACE/437body.htm

- 1 = Trace
- 2 = Trace to Light
- 3 = Light
- 4 = Light to Moderate
- 5 = Moderate
- 6 = Moderate to Heavy
- 7 = Heavy
- 8 = Severe

In accordance with AWC threshold guidelines, an icing event was considered to have occurred when icing intensities of category 4 or greater were reported in the PIREP data. All icing reports of category 4 or greater were accepted regardless of aircraft type. For an icing event with multiple latitudes and longitudes, i.e., a line segment, or dogleg in the case of three sets of latitudes and longitudes, the event was assigned to all 48 km grid blocks through which the line segment(s) passed. Line or dogleg segments over 300 mi (480 km) were, however, not used due to the likelihood of reporting errors. Aviation forecasters at AWC have observed through experience that segments over 300 mi are sometimes unreliable. In general, most line segments are reported by general aviation pilots in the low-band region at or below 15,000 ft. Above 15,000 ft, airline and military pilots usually give point reports of aircraft icing. As previously noted, national lightning location data were used to eliminate any icing events associated with thunderstorm activity. In effect, a value of zero was stored for all 48-km grid blocks where one or more cloud-to-ground flashes were reported during the hour. Grid blocks immediately adjacent to a thunderstorm area were also set to zero to reduce the possibility of contaminating the sample with convective icing events.

c. Predictor Sample

Atmospheric conditions that lead to aircraft icing are mesoscale in nature and are not resolvable at the grid spacing of the NGM. Icing conditions are most commonly found in clouds where supercooled liquid water (SLW) is present, i.e., where the temperature range lies between 0 deg C and -20 deg C. The threat of ice accumulation to aircraft passing through the supercooled layers is determined by the size and distribution of the cloud droplets and the speed and aerodynamic characteristics of the aircraft. Icing prediction is, therefore, a matter of identifying cloudy regions with the appropriate temperature range. In practice, forecasters have used the 850-mb temperature, 1000-500 mb mean relative humidity, and 700-mb vertical motion to delineate threat areas for icing (Schultz and Politovich 1992). Thus, the NGM predictors offered to the screening regression procedure are designed to identify large-scale synoptic flow patterns that are related to the occurrence of icing. This approach has been successfully employed in previous MOS developmental efforts to predict other mesoscale weather elements, e.g., clear-air turbulence (Reap 1996) and thunderstorms and severe local storms (Reap and Foster 1979). Table 1 lists the basic and derived predictors from the NGM that were offered to the screening regression procedure. Derived predictors include potential temperature, equivalent potential temperature, temperature-dew point spread, vertical velocity times relative humidity, equivalent potential vorticity (Rotunno and Klemp 1985), and height of freezing level. Stability indices in the form of the Total Totals index (Miller 1972), K index (George 1960), and lifted index were also included. The terrain-induced vertical velocities in Table 1 were included to account for the generation of SLW by orographic lifting. As shown by Modica et al. (1994), orographic lifting can be responsible for producing SLW at levels near 500-600 mb over the western mountains. Also included in Table 1 were several predictors originally developed for the prediction of clear-air turbulence (Reap 1996), i.e., the deformation and the TI1 and TI2 indices developed by Mancuso and Endlich (1966).

The deformation predictors are given by:

Shearing deformation = DSH = v/ x + u/ y

Stretching deformation = DST = u/ x - v/ y

Total deformation = DEF = (DSH2 + DST2)1/2

file:///V|/TPB/REPLACE/437body.htm

where u and v are the horizontal wind components. Deformation is a quantifiable kinematic predictor that acts to strengthen upper-level frontal zones by increasing the horizontal temperature gradients, thereby increasing the likelihood of the generation of SLW by frontal lifting. TI1 and TI2 are computed over specified layers and are given by:

$$TI1 = VWS \times DEF$$

$$TI2 = VWS \times (DEF + CVG)$$

where VWS is the vertical wind shear and CVG is the horizontal mass convergence computed for the specified layer as given by:

$$CVG = -(u/x + v/y)$$

The TI1 values are in units of 10^{-7} sec^{-2} and range in value from 0 to 15 units. When vertical wind shear is combined with deformation and horizontal convergence in the TI1 and TI2 indices, important predictors are created that simulate the nonlinear interactions among the three predictors and their relationship to aircraft icing. These predictors were selected in the final probability equations. Many of the predictors shown in Table 1 are interactive, or combined, predictors (Reap and Foster 1979), including the original formulations of TI1 and TI2 developed by Mancuso and Endlich (1966). Other interactive predictors in Table 1 include the vertical velocity, deformation, and vertical wind shear combined with various synoptic fields, i.e., relative humidity, temperature lapse rate, wind speed, and horizontal convergence. The function of the interactive predictors is partially to account for the particular, diverse, and probably nonlinear combinations of conditions that can lead to the occurrence of the predictand event. The selected variables are expected to interact with or complement one another in predicting the event. Previous studies have shown no clear consensus on the relative order of importance of many of the predictors in Table 1 as related to the occurrence of aircraft icing. In the present work, we are dealing with a very large developmental data sample; therefore, the MOS screening regression procedure should generate stable and reliable statistical relationships between the predictors and the occurrence of icing.

d. Unconditional Aircraft Icing Probability Equations

Linear screening regression and the MOS approach were used to develop forecast equations that give the unconditional probability of aircraft icing for both the warm (March 16 - September 30) and cool seasons (October 1 - March 15). Initially, 12-term forecast equations were developed for each region in Fig. 1 for the four valid periods (2-8, 8-14, 14-20, and 20-26 hours) following the 0000 and 1200 UTC initial data times. To enhance forecast consistency, a representative list of 12 predictors was assembled based on the individual predictor lists for the separate runs for each region. The screening regression procedure was then repeated to develop the operational equations by forcing selection of these 12 predictors, thereby, helping to ensure forecast consistency from one valid period to the next. The analysis of icing reports and forecast model fields was limited to the grid blocks within the contiguous U.S. landmass (Fig. 1); no oceanic grid blocks were used in the regression procedure.

The forecasts produced from the resulting equations represent the unconditional probability of aircraft icing intensities of category 4 or greater in 48-km grid blocks during the four 6-h valid periods. Each equation was developed from a generalized dataset created by combining data from all grid blocks for each region in Fig. 1. The total sample size for the East was about 1.2 million cases (2949 overland grid blocks times 409 sample days) for the 1988-90 cool seasons. For the West, the cool-season sample size was about 0.7 million cases (1728 blocks times 409 days). For the warm season, the sample size was 1.7 million cases for the East and 1.1 million cases for the West. These represent very large samples (588 days) which should result in stable and reliable forecast equations.

Icing frequency, or the fraction of 48-km grid blocks with icing intensities of category 4 or greater, was generally between 0.1% and 0.7% for the individual 6-h forecast projections during the warm and cool season developmental samples. Aircraft icing is a rare event relative to the total number of forecasts generated for the small 48-km grid blocks shown in Fig. 1. Predictand frequency and the resulting range

file:///V|/TPB/REPLACE/437body.htm

of forecast probabilities are also directly related to grid block size. Small grid blocks result in lower frequencies since a smaller geographical area is "verified" by a given occurrence of icing. Table 2 shows the 12 predictors in the cool-season icing forecast equations for the eastern and western U.S. for the low-band region at or below 15,000 ft for the four 6-h projections after 0000 and 1200 UTC. Predictors are listed in the order of importance in terms of their contribution to the cumulative reduction of variance. As shown in Table 2, the leading predictor for both East and West is relative humidity. In the East, the vertical stratification of temperature and moisture is of prime importance to the occurrence of SLW, followed by contributions from predictors that reflect atmospheric dynamics, i.e., 700-mb relative vorticity, 950-mb height, 500-mb equivalent potential vorticity, and the 300-mb vertical wind shear times wind speed. In the western U.S., contributions from relative humidity and temperature distributions are modified by contributions from terrain-induced vertical motions, moisture convergence, wind shear, wind speed, and the TI1 and TI2 indices, reflecting the importance of atmospheric dynamics related to the underlying topography in the West. Table 3 is similar to Table 2, except that it shows the 12 predictors for the high-band region above 15,000 ft. Predictors selected for the high-band equations were similar to those shown in Table 2 for the low band.

3. Verification

As previously noted, icing frequencies were less than 1% for the individual 6-h forecast projections resulting in a probability range of about 0 to 4% (0 to 1.4%) for the low-band (high-band) MOS forecasts. Therefore, for ease of use, probabilities for category 4 or greater icing were scaled (inflated) for both the low band and high band. As a result, the scaled probabilities for both bands roughly correspond to a range of 0 to 100%. Hereafter, use of the term "probability" refers to the scaled probability values. The reliability or bias of the operational icing equations was evaluated by producing forecasts on the dependent data and then computing frequencies for several icing probability categories, where the scaled values range from 0-10%, 10-20%,...etc. To compute the frequency for each of the scaled forecast categories, the total number of grid blocks for which icing was forecast in that category and for which icing intensities of 4 or greater were observed, was divided by the total number of daily forecasts or grid blocks in that category. For example, the reliability of the cool season probability forecasts for category 4 or greater icing for the 20-26 h projection for the low-band (high-band) regions is shown in Figs. 2 and 3, respectively. The data points are located at the average scaled forecast probability for each of the categories. The number of forecasts (plotted in thousands) is also shown next to each data point. The unlabeled diagonal line represents perfect forecast reliability or zero bias. Figures 2 and 3 indicate that the icing probability forecasts were reasonably reliable for the 1988-90 dependent data sample with a slight tendency to underforecast in the highest probability categories. Similar verification statistics were obtained for the remaining forecast projections in the dependent data sample. Based on our experience in testing other MOS forecast equations on dependent data, no significant degradat- ion is anticipated in the verification statistics for independent data samples. To further examine the usefulness of the probability forecasts to the operational forecaster, we produced categorical or yes/no forecasts of aircraft icing based on the grid block probabilities. The expected accuracy of such forecasts as a function of various scaled probability threshold values is indicated in Fig. 4 for category 4 or greater icing in the low-band. The threshold values are, in effect, scaled probability values that could be selected by the forecaster to delineate the regions where icing is expected to occur. Figure 4 contains several scores suggested by Donaldson et al. (1975). Table 4 shows the contingency table used in computing the scores. The scores computed are the probability of detection (POD), given by x/(x+y), the false alarm ratio (FAR), given by z/(x+z), and the critical success index (CSI), given by x/(x+y+z). Due to the relative rarity of icing and icing observations, most grid blocks contain no icing reports; hence, the FAR in Fig. 4 is uniformly high resulting in correspondingly low values for the CSI. The POD, therefore, is the primary score to be considered in this discussion. The probability forecast of category 4 or greater icing in Fig. 5, though for a different forecast interval, can be used to illustrate the effect of selecting one of the probability threshold values based on the POD in Fig. 4. If, for example, a threshold value of 20% (heavy line in Fig. 5) is selected from Fig. 4, then the area defined by this probability isoline would be expected, on average, to contain about 60% of the observed icing events, as shown by the POD in Fig. 4. Selection of an appropriate threshold value by the local forecaster is ultimately based on experience gained by using the probability guidance over an extended period of time.

file:///V|/TPB/REPLACE/437body.htm

4. Forecast Considerations

Predictand frequency and the resulting range of forecast probabilities are directly related to grid block size. Small grid blocks will automatically result in lower predictand frequencies, a limited range of forecast probabili- ties, a higher score for the FAR, and a lower score for the CSI. These trends occur since a smaller geographical area (and, consequently, a lower percentage of grid blocks) is "verified" by a given icing event. As a result, the NGM-based icing probability forecasts for the low band (high band) range between 0 and 4% (0 to 1.4%), considerably less than previous MOS probability forecasts, e.g., Reap and Foster (1979). The lower probability forecasts from the NGM-based icing probability equations are, in effect, a direct result of the relative rarity of aircraft icing and the small 48-km grid blocks used in equation development. As previously noted, the category 4 or greater icing probability forecasts for both low and high bands were scaled (inflated) to assist the forecaster in ease of pattern recognition. The MOS forecast for category 4 or greater icing in the low band shown in Fig. 5, for example, corresponds to contours indicating a scaled (actual) probability range of 0% to 65% (0% to 3.25%).

Significant diurnal variations in the magnitude of the probabilities from one 6-h interval to the next were found in the initial test forecasts due to the temporal variability in the reported icing events. Relatively low frequencies are reported at night, for example, during the 2-8 h interval after 0000 UTC and the 14-20 h interval after 1200 UTC (9 p.m. to 3 a.m. EST) when relatively few aircraft are aloft. In contrast, the highest icing frequencies are reported during the day for the 14-20 h interval after 0000 UTC and the 2-8 h interval after 1200 UTC (9 a.m. to 3 p.m. EST) when aircraft traffic is at a maximum. In effect, the icing forecasts give the probability of icing being reported during each of the forecast projections. To compensate for the pronounced diurnal variability, the forecasts for the 1400 to 2000 UTC (maximum reported icing frequency) and 0200 to 0800 UTC (minimum reported icing frequency) forecast projections were calibrated to ensure consistency with the magnitudes of the probability forecasts for the remaining forecast projections. The calibration procedure preserves the forecast patterns for the adjusted intervals and simply modifies the magnitudes to be consistent with those found in the preceding and following projections.

The operational forecasts are, therefore, not true probabilities since they have been scaled to provide sufficient magnitudes for objective analysis and display and calibrated to ensure consistency in the forecast magnitudes from one projection to the next. These modifications are justified on the basis that the observed frequencies of icing are not true observed frequencies since they depend directly upon the average number of aircraft aloft during any given projection. The modified forecasts should, therefore, be viewed as indices of icing occurrence rather than true probabilities. In any case, the areal patterns are of paramount interest to the forecaster. Continued daily use of the scaled and calibrated icing forecasts should allow the forecaster to develop a "feel" for the magnitudes and how they relate to the number and severity of observed aircraft icing. In effect, the magnitude of the icing forecast is not nearly as important as the ability to accurately delin- eate the potential areal extent of significant icing. In practice, the threshold values will be subjectively determined based on the day-to-day experience of operational forecasters at AWC in their preparation of operational AIRMETS and SIGMETS. Selection of appropriate threshold values should result in objectively determined areas of expected icing similar in size to those on manual products issued by operational forecasters.

The NGM-based MOS forecasts of aircraft icing should be operationally useful to the forecaster for several reasons. Use of lightning data, for example, to remove convectively-generated icing gives an improved definition of the icing predictand which should result in better statistical relationships with the NGM predictors. Use of relatively small (48 km) grid blocks allows the icing forecast equations to locate and define icing maxima more accurately, as shown, for example, by the narrow band across northern Illinois, Indiana, and Ohio shown in Fig. 5. Finally, the relatively large 3-year sample of predictor and predictand data should result in more stable and accurate forecast equations. As is the case with all MOS forecasts, however, the new NGM-based icing forecasts are highly dependent upon the accuracy of the NGM forecasts used as input. Therefore, the forecast guidance may have to be used with caution if the forecaster detects possible errors in the model predictions.

file:///V|/TPB/REPLACE/437body.htm

5. Graphics Products

The NGM-based MOS forecasts of aircraft icing are generated twice daily at NCEP. The output files are transmitted as NTRANS CGM metafiles to AWC in Kansas City, Missouri. The files are subsequently unpacked and processed for display on AWC's N-AWIPS communications system using the NTRANS graphical user interface. An example of the icing product, as displayed at AWC, is shown in Fig. 5. Within the context of the N-AWIPS system, the graphical icing products can be animated or looped as desired. Combined displays can also be generated with the icing forecasts and selected meteorological fields, such as the 850-mb relative humidity chart, etc., appearing on the same display. These options can be controlled by the forecaster to achieve maximum utility of the graphical icing index displays.

6. References

Donaldson, R. J., Jr., R. M. Dyer, and M. J. Kraus, 1975: An objective evaluator of techniques for predicting severe weather events. Preprints Ninth Conference Severe Local Storms, Norman, Amer. Meteor. Soc., 321-326.

George, J. J., 1960: Weather Forecasting for Aeronautics. Academic Press, 673 pp. Glahn, H. R., and D. A. Lowry, 1972: The use of Model Output Statistics (MOS) in objective weather forecasting. J. Appl. Meteor., 11, 1203-1211.

Hoke, J. E., N. A. Phillips, G. J. Dimego, J. J. Tuccillo, and J. G. Sela, 1989: The regional analysis and forecast system of the National Meteorological Center. Wea. Forecasting, 4, 323-334.

Krider, E. P., R. C. Noggle, and M. A. Uman, 1976: A gated wideband magnetic direction finder for lightning return strokes. J. Appl. Meteor., 15, 301-306.

Mancuso, R. L., and R. M. Endlich, 1966: Clear air turbulence frequency as a function of wind shear and deformation. Mon. Wea. Rev., 94, 581-585.

Miller, R. C., 1972: Notes on analysis and severe storm forecasting procedures of the Air Force Global Weather Central. Air Weather Service Tech. Rep. 200 (Rev.), U.S. Air Force, 102 pp.

Modica, G. D., S. T. Heckman, and R. M. Rasmussen, 1994: An application of an explicit microphysics mesoscale model to a regional icing event. J. Appl. Meteor., 33, 53-64.

Reap, R. M., 1996: Probability forecasts of clear-air turbulence for the contiguous U.S. NWS Technical Procedures Bulletin No. 430, NOAA, U.S. Dept. of Commerce, 15 pp.

_____ , and D. S. Foster, 1979: Automated 12-36 hour probability forecasts of thunderstorms and severe local storms. J. Appl. Meteor., 18, 1304-1315.

Rotunno, R., and J. Klemp, 1985: On the rotation and propagation of simulated supercell thunderstorms. J. Atmos. Sci., 42, 271-292.

Schultz, P., and M. K. Politovich, 1992: Toward the improvement of aircraft-icing forecasts for the continental United States. Wea. Forecasting, 7, 491-500.

Schwartz, B. E., 1996: The quantitative use of PIREPS in developing aviation weather guidance products. Wea. Forecasting, 11, 372-384.

Table 1. Basic and derived variables from the NGM offered as predictors to the regression analysis.

Predictor (level, if applicable)	
Temperature (850, 750, 700, 500 mb)	Vertical wind (speed) shear (300-500 mb) times wind speed (300 mb)
Temperature advection (850, 500 mb)	Vertical wind (speed) shear (300-500 mb) times total deformation (300 mb) plus wind speed (300 mb)
Potential temperature (850, 700, 500 mb)	Vertical wind (speed) shear (300-500 mb) times total deformation (300 mb) plus temperature lapse rate (300-500 mb)
Potential temperature difference (850-1000, 700-850, 500-700, 300-500 mb)	Vertical wind (speed) shear (950-500, 850-300 mb)
Equivalent potential temperature difference (850-1000, 700-850, 500-700, 300-500 mb)	Moisture Convergence (950, 850 mb)
Temperature minus dewpoint (1000, 850, 700, 500 mb)	Vorticity advection (500 mb)
Relative humidity (950, 850, 750, 700, 500 mb)	Relative vorticity (850, 700 mb)
Mean relative humidity (MRH) (1000-500 mb)	Equivalent potential vorticity (1000, 850, 700, 500 mb)
u horizontal wind comp (950, 850, 700, 500 mb)	Temperature lapse rate (850-1000, 700-1000, 500-700, 500-850, 700-850, 300-500 mb)
v horizontal wind comp (950, 850, 700, 500 mb)	Terrain-induced vertical velocity (500, 300 mb)
Wind speed (850, 700 mb)	Lifted index (1000, 850 mb)
Height (950, 850, 700 mb)	K stability index
Vertical velocity times relative humidity (700, 500, 300 mb)	Total totals stability index
TI1 index (850, 700, 500 mb)*	Height of freezing level
TI2 index (850, 700, 500 mb)*	Sine day-of-year
Layer TI1 index (850-950 mb)**	Cosine day-of-year
Layer TI2 index (850-950 mb)**	
Total deformation (850, 700, 500 mb)	
Layer total deformation (850-950 mb)	

* Wind deformation and convergence computed at the indicated level.
** Wind deformation and convergence computed over the layer.

Table 2. NGM predictors in cool season MOS forecast equations for category 4 or greater aircraft icing in the low-band for the 2-8 h, 8-14 h, 14-20 h, and 20-26 h projections following 0000 and 1200 UTC. Predictors are listed in order of importance.

Eastern U.S.	Western U.S.
700-mb relative humidity	850-mb relative humidity
700-mb relative vorticity	1000-500 mb mean relative humidity
300-500 mb temperature difference	850-950 mb TI2 index
Height of freezing level	500-mb terrain-induced vertical velocity
950-mb height	300-mb terrain-induced vertical velocity
850-mb relative humidity	850-mb TI1 index
500-mb equivalent potential vorticity	850-1000 mb temperature difference
700-850 mb equivalent potential temperature difference	950-mb moisture convergence
700-mb temperature minus dew point	850-mb moisture convergence
700-1000 mb temperature difference	850-mb temperature minus dew point
500-700 mb equivalent potential temperature difference	950-500 mb wind (speed) shear
300-mb vertical wind shear times wind speed	850-mb wind speed

Table 3. NGM predictors in cool season MOS forecast equations for category 4 or greater aircraft icing in the high-band for the 2-8 h, 8-14 h, 14-20 h, and 20-26 h projections following 0000 and 1200 UTC. Predictors are listed in order of importance.

Eastern U.S.	Western U.S.
700-mb relative humidity	1000-500 mb mean relative humidity
1000-500 mb mean relative humidity	700-mb wind speed
500-mb relative humidity	850-mb wind speed
Height of freezing level	850-mb TI1 index
500-mb vorticity advection	500-mb potential temperature
700-mb v wind component	850-mb TI2 index
500-mb temperature minus dew point	500-mb terrain-induced vertical velocity
850-mb TI2 index	950-mb moisture convergence
850-1000 mb equivalent potential temperature difference	700-mb vertical velocity times relative humidity
850-mb deformation	850-1000 mb equivalent potential temperature
500-mb v wind component	700-mb TI2 index
300-mb wind shear times deformation plus wind speed	850-mb moisture convergence

Table 4. Contingency table used in statistical analysis.

	Forecast		
Observed	ICING	No ICING	Total
ICING	x	y	x + y
No ICING	z	w	z + w
Total	x + z	y + w	x + y + z + w

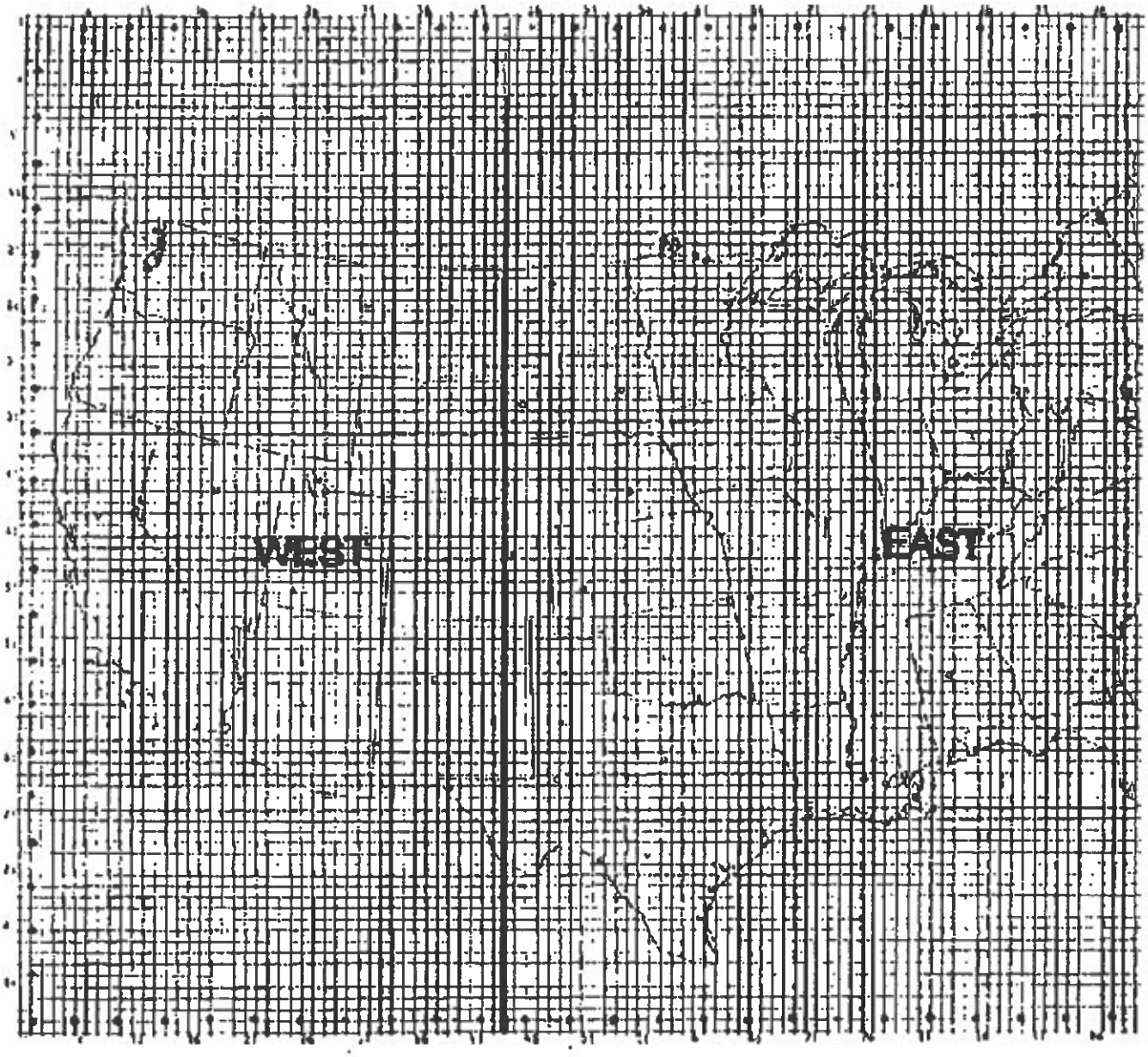

Figure 1. Development grid for MOS aircraft icing probability equations. Mesh length for 89x1 :s 48 km a: 60 deg north.

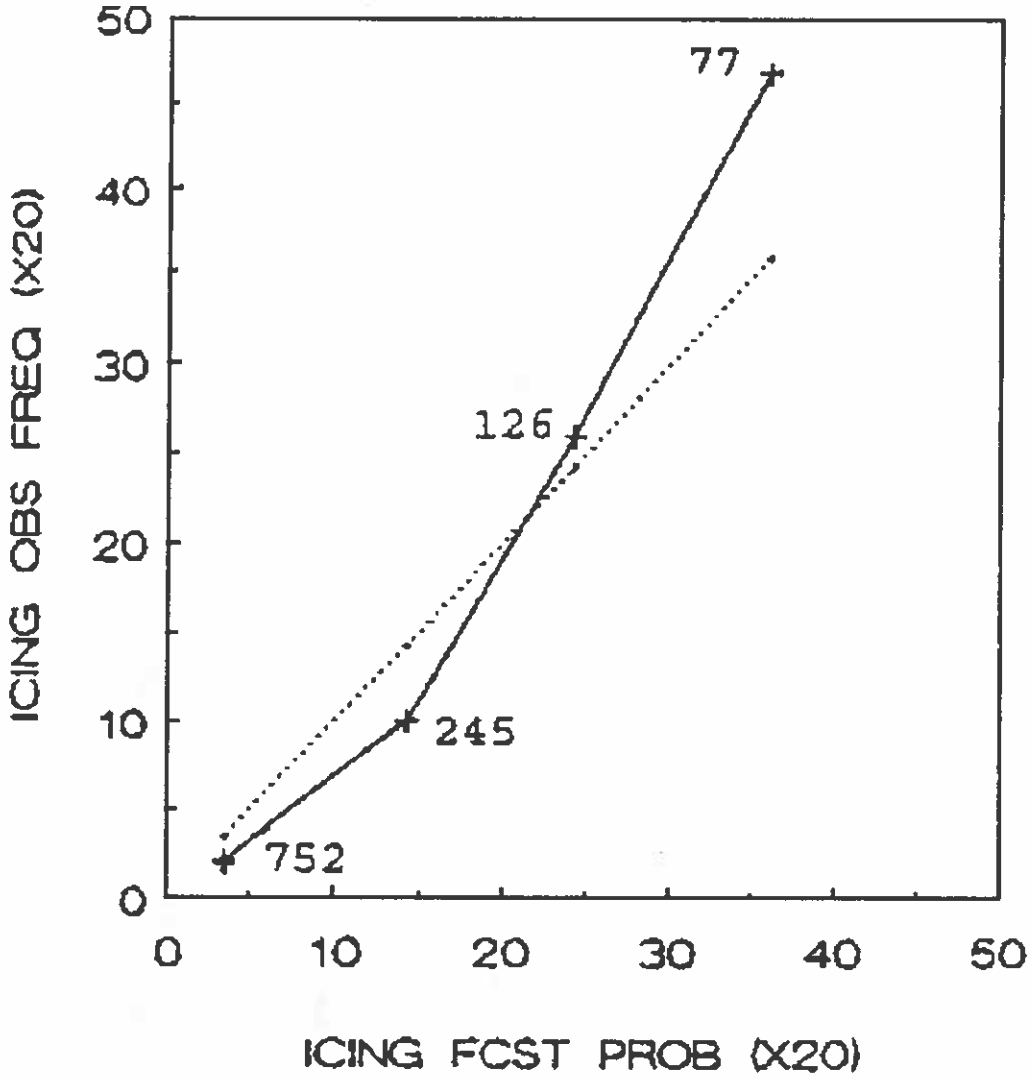

Figure 2. Reliability diagram for MOS aircraft icing probability forecasts for 20-26 h projection after 0000 UTC. The scaled forecasts are valid for the low-band region for the October 1 to March 15 cool season period during 1988-90. Number of cases (thousands) is plotted next to the data points for each category.

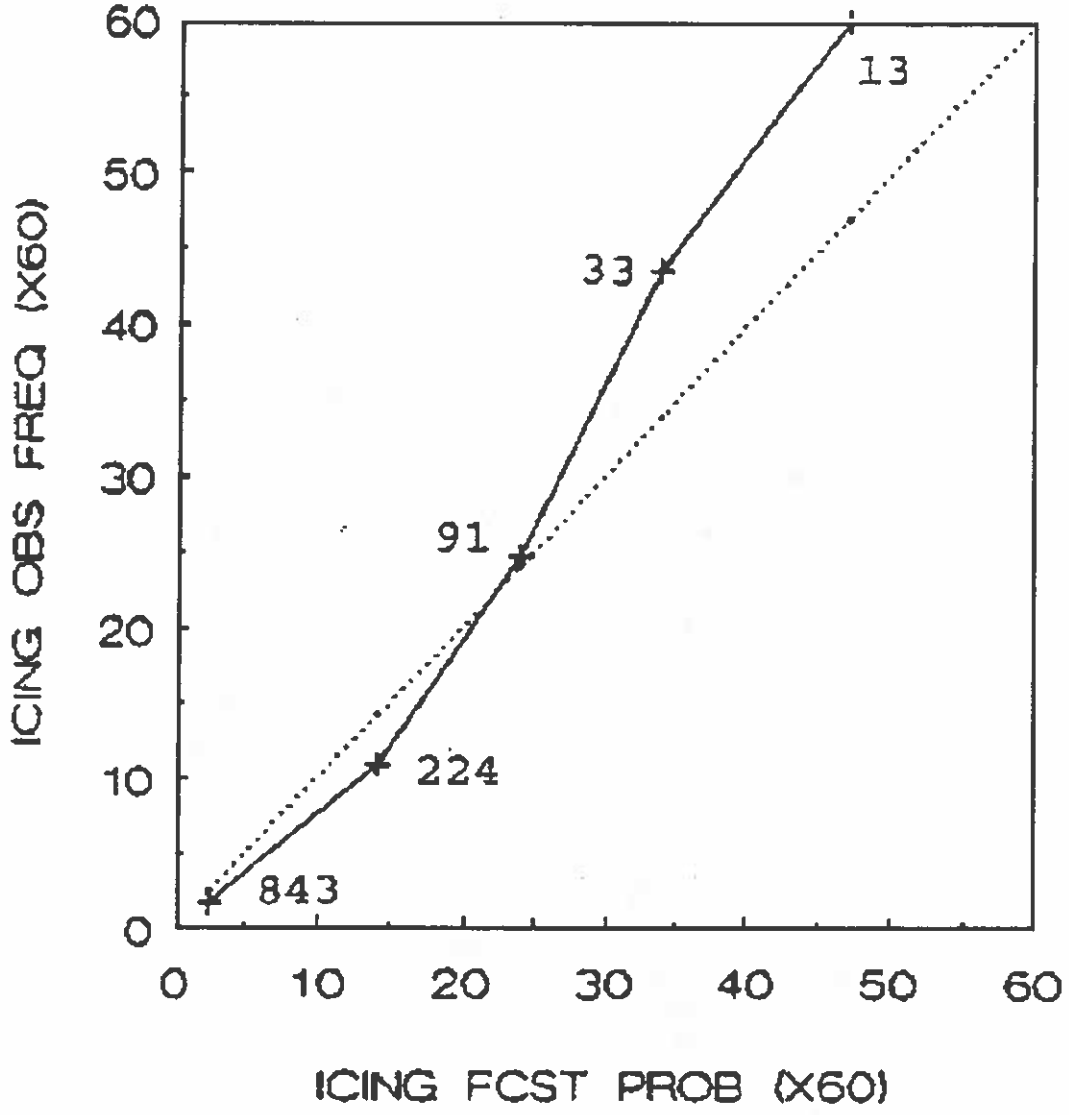

Figure 3. Same as Fig. 2, except for scaled high-band probability forecasts.

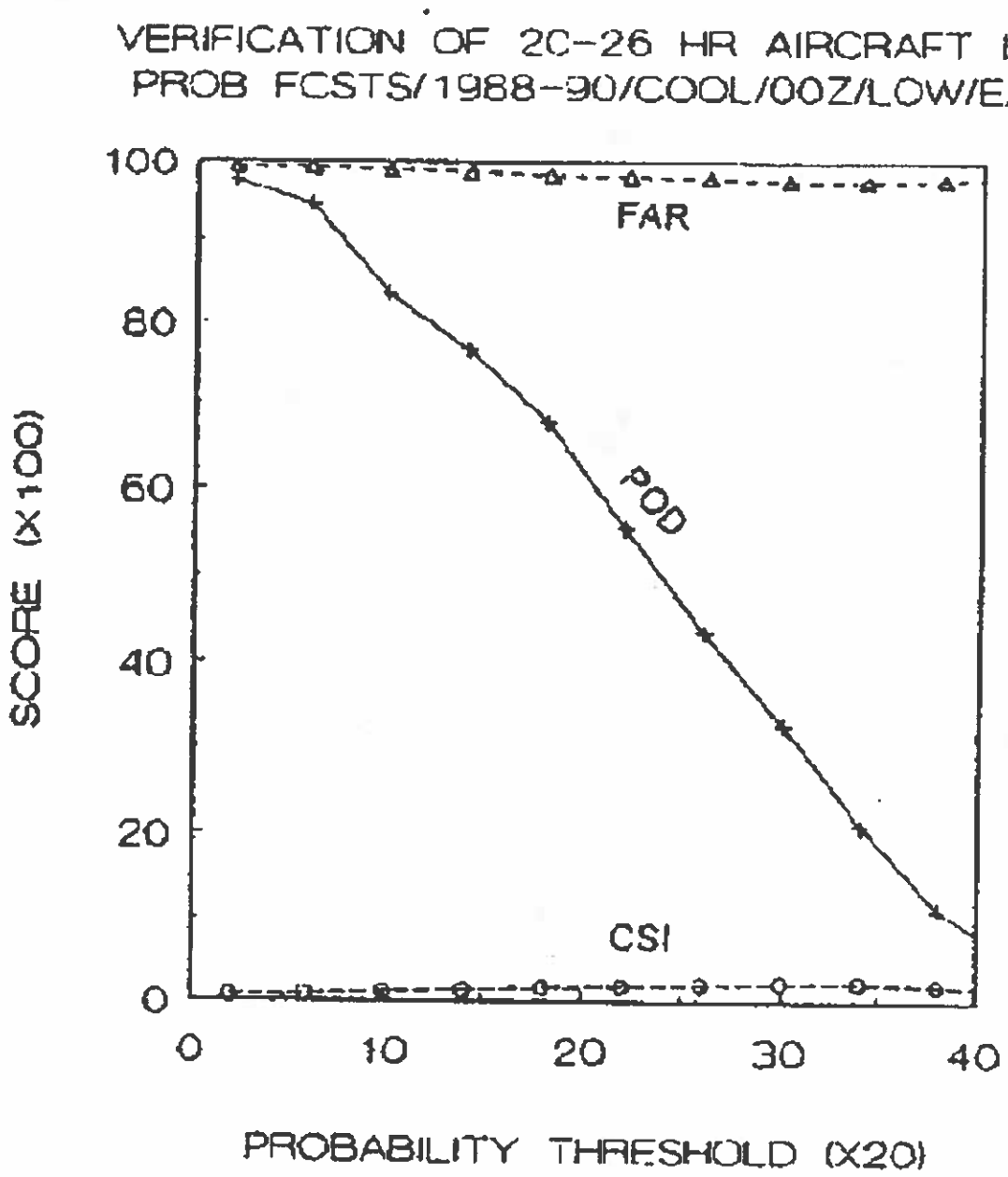

Figure 4. The critical success index (CSI), probability of detection (POD), and false alarm ratio (FAR) for categorical forecasts of category 4 (light-to-moderate) or greater aircraft icing based on various scaled (x 20) probability thresholds. Forecasts were for low-band region for 20-26 h projection after 0000 UTC during 1988-90 cool seasons.

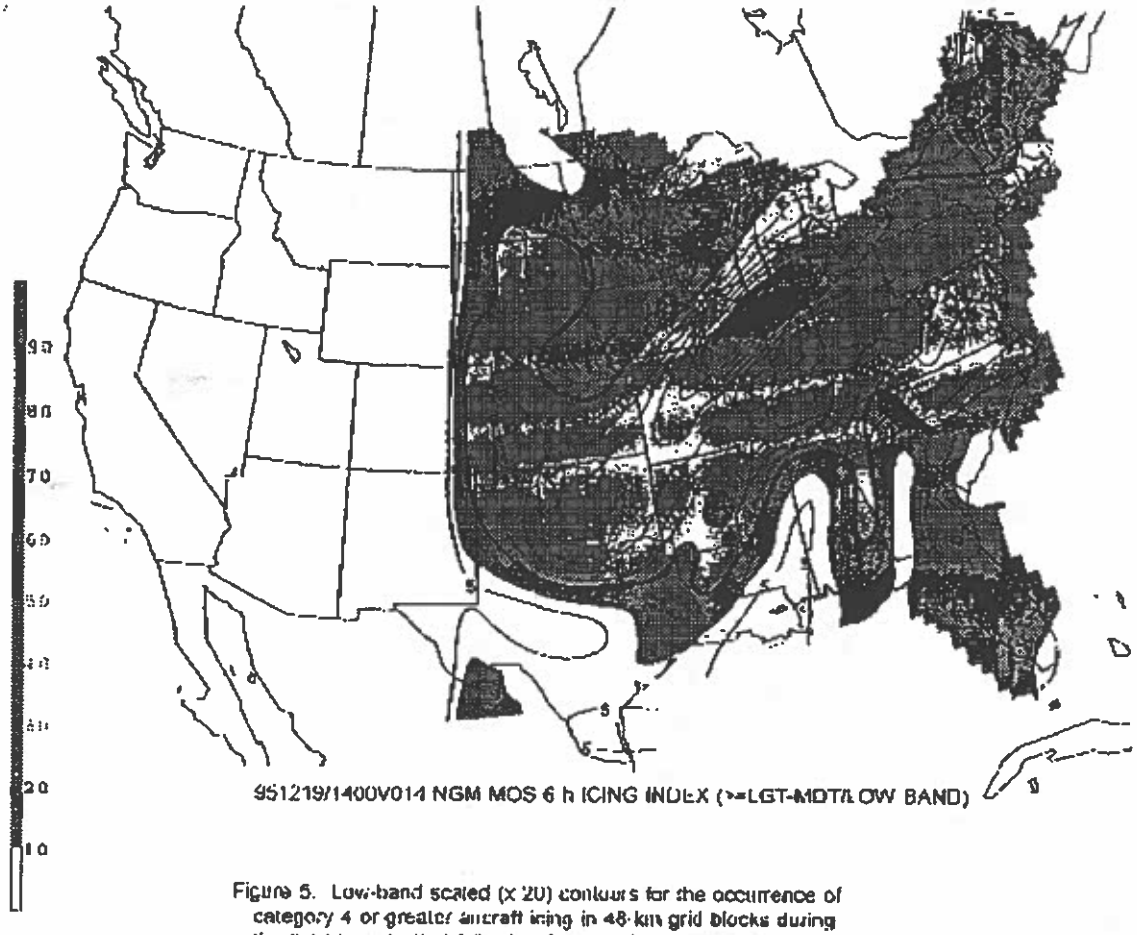

Figure 5. Low-band scaled (x 20) contours for the occurrence of category 4 or greater aircraft icing in 48-km grid blocks during the 8-14 h projection following 0000 UTC on December 19, 1995.